JCTC Journal of Chemical Theory and Computation

Article

pubs.acs.org/JCTC

Accurate Force Field Development for Modeling Conjugated Polymers

Kateri H. DuBay,[†] Michelle Lynn Hall,[†,∥] Thomas F. Hughes,[†,§] Chuanjie Wu,[‡] David R. Reichman,[†] and Richard A. Friesner*[,†]

[†]Department of Chemistry, Columbia University in the City of New York, New York, New York, United States

[‡]Schrödinger, New York, New York, United States

ABSTRACT: The modeling of the conformational properties of conjugated polymers entails a unique challenge for classical force fields. Conjugation imposes strong constraints upon bond rotation. Planar configurations are favored, but the concomitantly shortened bond lengths result in moieties being brought into closer proximity than usual. The ensuing steric repulsions are particularly severe in the presence of side chains, straining angles, and stretching bonds to a degree infrequently found in nonconjugated systems. We herein demonstrate the resulting inaccuracies by comparing the LMP2-calculated inter-ring torsion potentials for a series of substituted stilbenes and bithiophenes to those calculated using standard classical force fields. We then implement adjustments to the OPLS-2005 force field in order to improve its ability to model such systems. Finally, we show the impact of these changes on the dihedral angle distributions, persistence lengths, and conjugation length distributions observed during molecular dynamics simulations of poly[2-methoxy-5-(2′-ethylhexyloxy)-p-phenylene vinylene] (MEH-PPV) and poly 3-hexylthiophene (P3HT), two of the most widely used conjugated polymers.

1. INTRODUCTION

Conjugated polymers are of great interest for their potential use in photovoltaic devices and light emitting diodes. Although these polymers can be quickly and cheaply produced from abundant materials, significant advances in efficiency are required for them to compete economically with currently deployed solar cell and display technologies.[1] Future developments of novel applications for conjugate polymer materials will depend on a detailed understanding of the coupling between conformational and electronic properties.

Following synthesis, conjugated polymers are typically cast into thin films. The polymer's chemical structure as well as casting conditions influence polymer morphology within the film, and features of this morphology then influence the material's optoelectronic behavior.[2] Although the important role of polymer morphology in modulating this behavior is well-recognized, the precise morphology and its dependence on structural variations remains elusive. Molecular modeling provides a way to examine these effects at a level of detail that is generally unavailable experimentally. However, results from modeling will only be as good as the representation of the physical forces at work in these polymers.

Molecular force fields have historically been developed and refined for use with biomolecules, which generally do not contain extensive conjugation. In conjugated systems, the combined effect of shorter interatomic bond lengths and a bias toward planar configurations leads to unusually strong steric clashes, especially for conjugated bonds that link together ring moieties, such as those found in polyphenylene vinylene (PPV) and polythiophene (PT). These systems test the limits of current force fields; even small errors in the modeling of forces involved in bond-stretching, angle-bending, torsion rotations, and steric interaction can result in inappropriate modeling, especially of the energies involved in rotations about the inter-ring torsions. However, accurate modeling is particularly important for those dihedral angles since the inter-ring torsion degree of freedom is one of the most influential in terms of both the polymer's large-scale fluctuations and folding as well as the length over which its electrons delocalize. Thus, appropriate modeling of the arrangement and nature of the material's chromophores depends upon an accurate representation of the forces influencing these inter-ring bond rotations.

We begin this paper by discussing the effects of inadequate potentials in section 2. Then, in section 3, we calculate and justify the use of LMP2-derived potential energy surfaces for the inter-ring torsions of a series of substituted stilbene and bithiophene derivatives, which constitute the basic dimers of the ubiquitous polyphenylene-vinylene (PPV) and polythiophene (PT) polymers. After demonstrating the inability of the standard OPLS-2005 potential to adequately reproduce the LMP2 curves in sections 4 and 5, we then test and discuss a variety of adjustments to the OPLS-2005 potential in sections 6 and 7. Finally, in section 8, we consider the influence of our adjustments on sampled torsion angle distributions, persistence lengths, and conjugation length distributions during molecular dynamics simulations of poly[2-methoxy-5-(2′-ethylhexyloxy)-p-phenylene vinylene] (MEH-PPV) and poly 3-hexylthiophene (P3HT).

2. EFFECTS OF INACCURATE POTENTIALS

Modeling conjugated polymers with classical force fields that were designed primarily for nonconjugated systems may yield unphysical results along several dimensions. In general, energy minima may be located inaccurately, the shapes of energy basins may be too narrow or too wide, and energy barriers may

Received: March 1, 2012
Published: October 10, 2012

be over- or underestimated. In particular, errors may be expected in the following: close steric interactions, bending and stretching under strain, rotations around conjugated bonds, planarity of conjugated segments, and $\pi-\pi$ stacking interactions. As a result, errors may arise in the modeling of optimal conformations and molecular fluctuations as well as in the modeling of the kinetically dominated folding, self-assembly, and electronic behaviors of conjugated polymers and their aggregates. In addition, we consider here only fixed charge force fields; thus errors resulting from the failure to explicitly treat polarization effects may also be expected.

By far, the largest errors that existing force fields manifest when applied to conjugated polymers reside in the potential energy curves around torsional bonds connecting aromatic moieties. The most straightforward approach to reducing these errors is to fit torsional coefficients to an accurate quantum chemical potential surface. Such an approach can work reasonably well if the goal is to model one specific polymer. However, in modeling conjugated polymers, we seek to assist in the design and optimization of new polymeric materials with specific functional properties. This task may require the modeling of thousands of chemical variants of the aromatic cores, linker regions, and side chains, but performing accurate quantum chemical calculations for each of these variants and then refitting the torsional parameters appropriately would entail an enormous and arguably prohibitive amount of work. Hence, the goal of conjugated force field development must be to develop a model and set of parameters that are transferable and can be used to model the entire set of envisioned polymers. Lack of transferability is a defect that goes beyond the manifestation of large errors for a single polymeric chemistry (which could be repaired by refitting torsions); it is indicative of problems within the broader scope of the force field as applied to the types of chemistry under study. In the present case, the key challenge is to properly represent conjugation effects while at the same time balancing those effects against the steric interactions that arise from side chain clashes. As we shall see below, even the best performing current force fields experience difficulties in this regard. In this work, we suggest some approaches to solve the problem and demonstrate that, at least for the set of examples considered here, these approaches are transferable and display considerable success in reducing the errors to acceptable levels. Beyond transferability, a second (and more subtle) problem is scalability; will an approach that works for a small number of anecdotal examples enable the development of a larger and more comprehensive set of parameters that exhibit a similar level of error control and transferability across a broader range of chemical functionality? We argue that the improvements proposed below are readily scalable to broad chemical coverage and thus provide a path forward toward robust and accurate modeling of conjugated polymer systems.

3. LMP2-CALCULATED POTENTIALS

To obtain accurate torsional potentials for complex molecules, it is necessary to fit the torsional profiles to energies obtained from a suitable level of quantum chemical calculation. In the present paper, we employ localized second order Moller–Plesset perturbation theory (LMP2),[3,4] using the cc-pVTZ (-f) basis set of Dunning and co-workers,[5−8] as implemented in the Jaguar suite of ab initio electronic structure programs.[9] We have used LMP2 calculations extensively in previous development efforts, for example in constructing a refined version of the OPLS force field for peptides and proteins,[10] which has been in use in a variety of academic and industrial laboratories for the past 10 years. LMP2 calculations are highly efficient (scaling approximately as N^3)[3] but deliver good accuracy for conformational energy differences. For example, in ref 3, conformational energy differences for 36 small molecules are evaluated at the LMP2 level and compared with canonical MP2 and experimental results; the mean unsigned error and RMSD compared to experimental results are a few tenths of a kilocalorie per mole, and the results are also quite similar to the canonical MP2 results, although somewhat closer to experimental results. Benchmark results for the computation of hydrogen bond energies have also yielded excellent results[11] when compared with CCSD(T) data and (for N-methyl acetamide) when used to develop a polarizable force field and compared with experimental liquid state properties. When a substantial but incomplete basis set is used (as is the case here), LMP2 provides some advantages as compared to canonical MP2 in avoiding problems with basis set superposition error.[3] Finally, recently published free energy perturbation (FEP) calculations[12] of the binding affinity difference between two ligands to the protein thrombin resulted in a qualitatively superior match to experimental values when LMP2 data were used to develop new torsional potentials, as contrasted with results obtained with an older potential function in which some torsions were not properly fit to quantum chemical data. These results are quite relevant to the present problem concerning conjugated polymers, as the ligands in question have torsions between two aromatic rings which are analogous to those investigated here.

Although we have previously found the LMP2/cc-pVTZ(-f) level of quantum chemistry to provide good accuracy for force field development parameters,[12] we compared the LMP2 and canonical MP2 results for a few specific systems under study in the present paper in order to investigate any possible issues associated with this component of our approach. Table 1 shows the relative energies for the inter-ring torsions of stilbene and methyl-substituted stilbene (see Figure 1) at three points on the torsional surface (with the energy of the 180° state set to zero in all cases), using the LMP2/cc-pVTZ(-f), MP2/cc-pVTZ (-f), and MP2/cc-VQZ levels of theory.

Table 1. Relative Energies (in kcal/mol) of Stilbene Torsion Angles, As Computed Using LMP2 and MP2

torsion angle	stilbene α, R = H	stilbene β, R = H	stilbene β, R = Me
	LMP2/cc-pVTZ(-f)		
0	3.63	0.07	1.79
90	37.05	3.96	2.90
180	0.00	0.00	0.00
	MP2/cc-pVTZ(-f)		
0	2.48	0.01	1.12
90	35.81	3.94	3.13
180	0.00	0.00	0.00
	MP2/cc-pVQZ		
0	2.76		
90	36.06		
180	0.00		

The rotation around the α torsion of stilbene provides a particularly good test case. In our calculations, the 90° configuration is far above the 180° state in energy (in fact, it represents the magnitude of the rotation barrier), and the

dx.doi.org/10.1021/ct300175w | J. Chem. Theory Comput. 2012, 8, 4556−4569

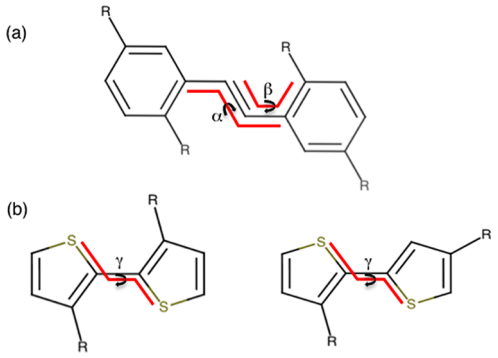

Figure 1. (a) Stilbene with two substituted R groups. The torsions of interest, α and β, are marked by the arrows, and the atoms defining them are highlighted by the red bars. In this study, we consider R = H, Me (methyl), Et (ethyl), OH (hydroxyl), OMe (methoxy), OEt (ethoxy), and OiPr (isopropoxy). (b) 3,3′- (left) and 3,4′- (right) disubstituted bithiophenes. The torsion of interest, γ, is again marked by an arrow, and the defining atoms are indicated by the red bars. For bithiophene, we consider R = H, Me, Et, and iPr (isopropyl). Note that no R-group atoms are highlighted by the red indicator bars.

LMP2 and MP2 results can be considered to be in excellent agreement, with the difference unlikely to affect physical or chemical properties in any significant way. The 0° state is an alternative minimum of the system, and the energy difference here, 1.1 kcal/mol, though not particularly large, is noticeable. To investigate further, we increased the basis set size for the MP2 calculations. As argued in ref 3, the MP2 calculations are more likely to be subject to basis set superposition error, which would imply an overstabilization of the 0° state as compared to the 180° state. This is consistent with the MP2 results for the 0° state being 1.1 kcal/mol lower in relative energy than the LMP2 results. When the larger QZ basis set is used, one would predict that the basis set superposition error would be reduced, and therefore the difference between the LMP2- and MP2-calculated relative energies of the 0° state would decrease. This is in fact what is observed; with the use of the QZ basis, this difference is reduced to 0.8 kcal/mol. This trend is likely to continue with basis set size, and the final value for complete basis set MP2 might well be within 0.5 kcal/mol of the LMP2 result, closer to the LMP2 value than the triple-ζ MP2 value. It is unrealistic to expect an accuracy of better than 0.5 kcal/mol for relative energies in practical applications, given present-day computing resources and available quantum chemical technologies. Furthermore, it might not be useful as there are likely comparable errors in free energy that are present in the simulation algorithms, which cannot yet converge polymer simulations to a high precision. Consequently, our conclusion is that, consistent with the results we discussed previously for biomolecular simulations, the LMP2/cc-pVTZ level of theory is

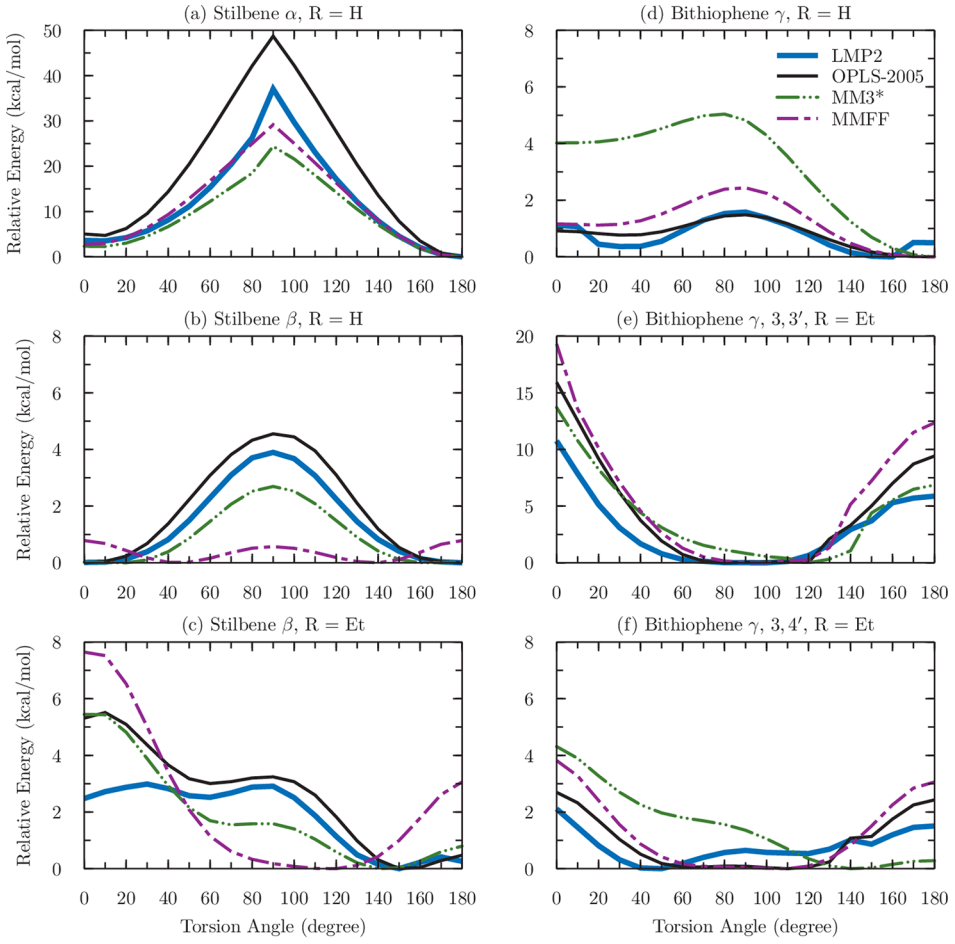

Figure 2. Comparison of torsion potentials calculated by LMP2, OPLS-2005, MM3*, and MMFF for (a) the α torsion (see Figure 1) of unsubstituted stilbene, (b) the β torsion of unsubstituted stilbene, (c) the β torsion of ethyl-substituted stilbene, (d) the γ torsion of unsubstituted bithiophene, (e) the γ torsion of 3,3′-diethyl-bithiophene, and (f) the γ torsion of 3,4′-diethyl-bithiophene.

dx.doi.org/10.1021/ct300175w | J. Chem. Theory Comput. 2012, 8, 4556−4569

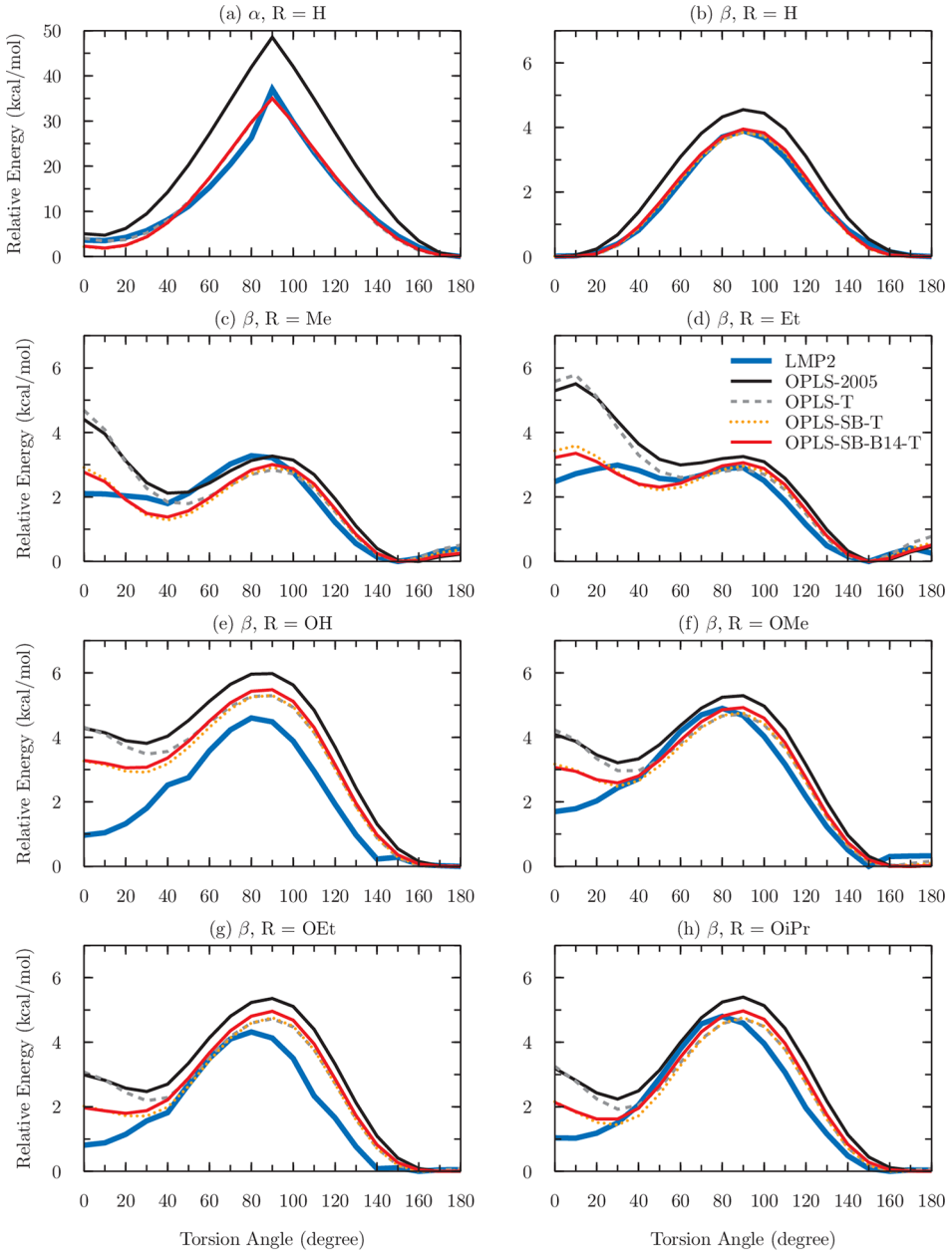

Figure 3. Comparison of LMP2 and various OPLS-2005 potentials for disubstituted stilbenes. (a) The potential around the α torsion angle (see Figure 1) for unsubstituted stilbene. (b–h) The potential around the β torsion angle for various R-substituted stilbene species: (b) R = H, (c) R = Me, (d) R = Et, (e) R = OH, (f) R = OMe, (g) R = OEt, and (h) R = OiPr.

suitable for our purposes, providing a combination of relatively low computing costs with an acceptable level of accuracy.

The torsional potentials of bithiophene and stilbene and their derivatives were therefore calculated at the LMP2/cc-pVTZ(-f)//B3LYP/6-31+G** level. This was achieved by sampling the torsion of interest (see Figure 1) at 10° intervals from 0 to 180° while optimizing all remaining degrees of freedom. For stilbenes, both α and β angles were examined, although α was examined only for the unsubstituted stilbene. Since the majority of PPV backbone linkages are in the *trans* configuration, and the barrier to rotation is quite high, α remained in this configuration ($\alpha \approx 180°$) during the minimizations as β was sampled at various dihedral angles. For bithiophenes, the sole inter-ring torsion, γ, was considered for unsubstituted as well as 3,3′- and 3,4′-disubstituted species. 3,4′-Disubstituted bithiophenes are representative of the polymer linkages in regioregular polythiophenes, while regiorandom polythiophenes contain 3,3′- and 4,4′-disubstituted bithiophene moieties. 4,4′-Disubstituted bithiophenes are not considered as they lack the more severe steric clashes present in 3,3′- and 3,4′-disubstituted bithiophenes and are presumably more amenable to treatment with the unmodified OPLS force field.

All geometries were initially optimized at the B3LYP/6-31+G** level since B3LYP is known to give good geometries at a reasonable computational cost compared to other methods. Subsequently, single-point energy calculations were performed at the LMP2/cc-pVTZ(-f) level. This level of theory was chosen as it gave good agreement with the *ab initio* results reported by Raos et al. for bithiophene[13] and Kwasniewski et al. for stilbene.[14] We assumed that this good agreement for stilbene and bithiophene would be transferable to function-

dx.doi.org/10.1021/ct300175w | J. Chem. Theory Comput. 2012, 8, 4556–4569

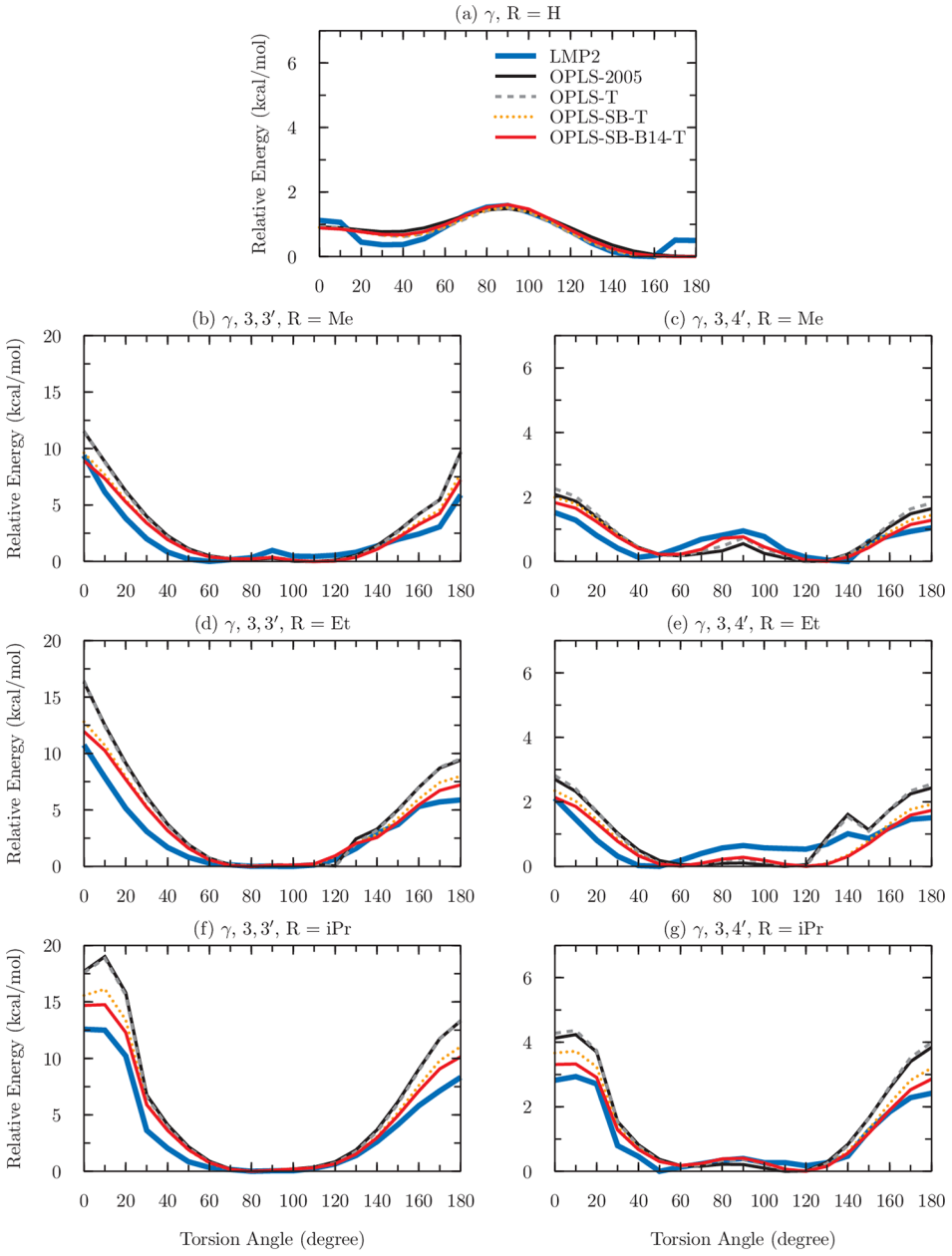

Figure 4. Comparison of LMP2 and various OPLS-2005 potentials for disubstituted-bithiophenes. (a) The potential around the γ torsion angle (see Figure 1) for unsubstituted stilbene. (b–g) The potential around the γ torsion angle for various disubstituted bithiophene species: (b) 3,3′-dimethyl-bithiophene, (c) 3,4′-dimethyl-bithiophene, (d) 3,3′-diethyl-bithiophene, (e) 3,4′-diethyl-bithiophene, (f) 3,3′-diisopropyl-bithiophene, and (g) 3,4′-diisopropyl-bithiophene.

alized stilbenes and thiophenes as well. Energies were computed every 10° between 0° and 180° (see Method Details). These results are shown in Figures 2, 3, and 4, where the thick blue lines represent the LMP2 results.

Stilbene and bithiophene may be considered as dimer model systems of PPV and PT systems, respectively. It is important to address the transferability of results derived with these dimer model systems to the study of full-length PPVs and PTs. Crystal structures of both PPVs and PTs show these polymers in roughly planar conformations.[15,16] Our calculations on stilbene certainly agree with the experimental results, where minima are located at 0° and 180° (*cis*-planar and *trans*-planar, respectively). (See LMP2 curve in Figure 3b.) However, for bithiophene, we witness minima at approximately 40° and 150° (*cis*-distorted and *trans*-distorted, respectively, see Figure 4a), not 0° and 180° as might be suggested by the observation of planar geometries in crystal structures.

Darling and Sternberg[17] have published an extensive study testing the transferability of *n*-mer model systems, where n = 2, 4, ..., 14, to full-length PTs. In agreement with our results, they find that dimers preferentially adopt distorted, instead of planar, minima. Notably, this is in disagreement with the torsions seen in crystals of longer PTs. They also find that increasing the size of the model *n*-mer system to $n \geq 4$ produces a qualitative change in the potential energy profile, and the minima are now at the planar, not distorted, conformations, in agreement with what is found in the crystal structures of PTs. Naïvely, this suggests that dimers produce results in qualitative disagreement with the crystal structure, as the dimers prefer distorted conformations while the polymers in crystals adopt planar

dx.doi.org/10.1021/ct300175w | J. Chem. Theory Comput. 2012, 8, 4556–4569

conformations. If true, one would conclude that the strict use of dimers is insufficient to model systems of longer PTs. However, it is important to note that Darling and Sternberg used a different level of theory (B3LYP/6-311G(d,p)//B3LYP/3-21G*) than that employed here. They note that, when optimizations are performed in bases larger than 3-21G*, all *n*-mers adopt distorted minima, in contrast to the planar minima obtained with 3-21G*.

Finally, in performing their scans on *n*-mers with $n \geq 4$, Darling and Sternberg fixed all γ dihedral angles (except the one under investigation) in their planar conformations, suggesting that they have located local, rather than global, minima. To test this, we have also performed scans on the 4-mer at the LMP2/cc-pVTZ(-f)//B3LYP/6-31+G** level of theory, since, as mentioned above, this combination gives good agreement with previously reported *ab initio* results.[13] Here, we varied all three γ torsions, and we were able to reproduce Darling and Sternberg's results. Indeed, we find that if all torsions are held fixed in their planar conformations while varying only the central torsion, overall planar conformations for the 4-mer are preferred over distorted conformations. Importantly, however, we also found that varying all torsions, not just the central torsion, gives a global minimum wherein all torsions prefer to adopt the *cis*-distorted over *cis*-planar conformation. Further, the *trans*-planar conformation is only 0.5 kcal/mol higher than the *trans*-distorted conformation, a value well within the error for such a level of theory.

Our results are in qualitative agreement with those of Darling and Sternberg, and both sets of results suggest that these polymers adopt distorted, not planar, geometries natively. Stated another way, as both dimers and 4-mers adopt nonplanar minima (within the error of the method employed to study these torsions), we posit that nonplanar minima are not unique to dimers but are likely be a feature of *n*-mers in general. This further suggests that crystal packing induces the planarity observed in crystal structures. Importantly, the dimers appear to be accurately capturing the nonplanar nature of the minima in these longer 4-mer systems. Thus, in contrast to Darling and Sternberg, we argue that dimers represent an appropriate model system for the study of PTs, as they reproduce the qualitative behavior of larger *n*-mers at the LMP2/cc-pVTZ(-f)//B3LYP/6-31+G* level while requiring only a fraction of the computational cost. For this reason, all parametrizations reported herein were performed using dimers.

4. OPLS-2005-CALCULATED POTENTIALS

Previous studies on conjugated polymers have generally made use of either the OPLS (Optimized Potentials for Liquid Simulations[18,19]) or the MM3 potentials.[16,19−22] MM3 provides additional terms and iterative bond order calculations that are not available in OPLS, but the additional computational costs do not appear to be justified. In fact, work by Marcon and co-workers has demonstrated that potentials based on OPLS-2005 outperformed those based on MM3, and more recent refinement and modeling efforts have shifted to OPLS-based potentials.[16,23,24]

Our initial investigations confirmed that OPLS-2005, an OPLS-AA force field[18] similar to OPLS-2003[19] but with additional parameters, provides a good starting representation of the inter-ring torsion potentials for stilbene and bithiophene. Figure 2 shows the superiority of OPLS-2005 over MM3*[20,25] and MMFF[26] in reproducing the potentials derived from LMP2 for a subset of the torsions we consider here. MM3*, while performing reasonably well in Figure 2a, b, and e, greatly overestimates the energies for torsions of less than 90° in Figure 2c, d, and f. MMFF performs reasonably well in Figure 2a, d, e, and f (although not as well as OPLS-2005 in these last three cases); however, the locations of its minima in Figure 2b and c are qualitatively incorrect. Overall, OPLS-2005 best reproduces the LMP2 results, especially considering that its overestimate of the barrier in Figure 2a can be easily corrected with softened torsion parameters.

Even though OPLS-2005 performs reasonably well, there are significant limitations to its accuracy (see Figures 2, 3, and 4). As a result, various optimizations have been made to OPLS for the study of oligothiophenes. However, until recently, the goal was to design a force field specific to each oligomer under investigation.[21,23] The most recent of these optimizations instead aims to improve OPLS's ability to model a wide range of oligothiophenes by focusing on crystalline oligothiophenes.[16] In this work, Moreno and co-workers reassigned electrostatic charges and refit various dihedral potentials to better reproduce known crystal configurations. However, the inter-ring torsion potential was optimized for a quarterthiophene without any side chains,[16] as was also the case in work done to optimize the AMBER force field for polythiophenes.[27] As a result, these studies do not address the problems we discuss herein, namely the inaccuracies that emerge upon side-chain substitution.

5. COMPARISON OF LMP2 AND OPLS-2005 POTENTIALS

Stilbene Derivatives. There is a striking difference between the resulting plots from unsubstituted stilbene (Figure 3a and b) and its substituted derivatives (Figure 3c−h). For unsubstituted stilbene, the difference between the two curves for the α angle is substantial, with OPLS-2005 overestimating the LMP2-derived barrier height at 90° by 11.9 kcal/mol. For the β angle, the overestimation is modest, just 0.7 kcal/mol at the barrier. However, both these discrepancies are symmetric around 90°, making them amenable to simple adjustments in the standard OPLS-2005 torsion parameters (see below). In contrast, the differences between the two potentials for the substituted stilbenes are less symmetric and consistently show the greatest discrepancy around 0−10°. It is precisely at these angles that the competition between steric clashes (intensified by the short length of the conjugated single bond) and the conjugation-induced planarity is most severe. In the *trans* configuration of α, β angles close to 180° avoid this problem, as the substituted group is in close contact with a hydrogen atom instead of the carbon atom it encounters at 0°. Interestingly, increasing the bulkiness of the substituent group, for example from methyl to ethyl and finally to isopropyl, does not necessarily increase this discrepancy. A quantitative comparison of the different potential energy curves can be seen in Table 2, where half of the structures have root-mean-square deviation (RMSD) values larger than 1.0 kcal/mol.

Bithiophene Derivatives. The comparison between LMP2- and OPLS-2005-calculated potential energy curves for unsubstituted bithiophene can be seen in Figure 4a. Within chemical accuracy (typically taken as errors ≤1 kcal/mol), the two approaches result in essentially the same curve. When considering the disubstituted molecules, however, substantial differences emerge, particularly for the 3,3′-disubstituted species. (See Figure 4b−g.) For these molecules, near-planar configurations where the γ angle is close to *either* 0° *or* 180° result in substantial error; unlike the stilbene derivatives, where

dx.doi.org/10.1021/ct300175w | J. Chem. Theory Comput. 2012, 8, 4556−4569

Table 2. RMSD between LMP2- and OPLS-Calculated Potential Energy Curves (in kcal/mol)

structures	OPLS-2005	OPLS-T	OPLS-SB-T	OPLS-SB-B14-T
		stilbenes		
α, R = H	8.47	1.29	1.51	1.49
β, R = H	0.54	0.10	0.08	0.11
β, R = Me	0.79	0.84	0.43	0.38
β, R = Et	1.16	1.18	0.39	0.34
β, R = OH	1.75	1.43	1.08	1.18
β, R = OMe	0.97	0.87	0.54	0.54
β, R = OEt	1.22	0.95	0.67	0.76
β, R = OiPr	0.97	0.78	0.49	0.52
		bithiophenes		
γ, R = H	0.26	0.21	0.22	0.23
γ, R = Me, 3,3′	1.61	1.60	0.95	0.82
γ, R = Et, 3,3′	2.42	2.39	1.38	1.13
γ, R = iPr, 3,3′	3.06	2.98	1.79	1.31
γ, R = Me, 3,4′	0.40	0.44	0.30	0.24
γ, R = Et, 3,4′	0.58	0.59	0.42	0.38
γ, R = iPr, 3,4′	0.71	0.76	0.41	0.25

the substituted group only makes close contact with a hydrogen in the 180° configuration, the substituted groups in bithiophene-derivatives make close contact with a bulkier sulfur atom. Naturally, the problem is exacerbated in the 3,3′-disubstituted species, as in these cases, the substituted moieties come into even closer contact with each other at configurations close to 0°. In general, increasing the bulkiness of the substituent group does increase the discrepancy for these bithiophene derivatives (see Table 2). Again, the OPLS-2005-calculated energies of several of these structures have a RMSD of greater than 1.0 kcal/mol from the LMP2-computed energies.

Consequences for Polymer Modeling. These results give a comprehensive picture of the substantial errors in the torsional potential that arise when utilizing the OPLS-2005 force field to model conjugated polymers. These large discrepancies indicate that for both stilbene and bithiophene derivatives, such as the commonly used polymers MEH-PPV and P3HT, sampling with the standard OPLS-2005 potential would significantly bias the results away from the appropriate kinetics and equilibrium distributions suggested by our LMP2 calculations. The location of the global minimum within the torsional potential is generally well-approximated by OPLS-2005. However, the barriers are typically overestimated and, in the stilbene derivatives, the local minimum that is present near 0° in the LMP2-derived potential is often modeled as a maximum in the OPLS-2005-derived version. These polymers are typically cast into thin films, where the degree of ordering and time scale of fluctuations greatly influence the electronic behavior of the film. This casting is a nonequilibrium process, and the kinetics of film formation will largely determine the final morphologies. We therefore consider physically realistic barriers to be vital in order to accurately model the folding, assembly, and electronic behavior of these molecules in the condensed phase. In addition, the quality of the OPLS-2005 potential varies significantly with changes to the side chains, rendering it less useful for comparing behaviors between structural variants of these polymers.

6. OPLS POTENTIAL ADJUSTMENTS

6.1. Torsion Adjustments. Upon first examination, it may appear that we can simply make adjustments to the torsional potential in order to fix these discrepancies. However, a closer look at Figure 1 suggests otherwise. The thick red bars highlight the four atoms that define each dihedral angle, making it clear that, for the torsions under consideration, no atoms from the substituted moieties are part of these four-atom sets. As a result, any torsional adjustments we could make to improve the potentials for substituted stilbene and bithiophene would then, by necessity, denigrate their performance for the unsubstituted species. Due to the substantial differences we observe between the unsubstituted and substituted molecules (see above), it seems unlikely that such an approach would be able to resolve the problems that occur when computing minimized energies for the near-planar configurations of these substituted species.

Nevertheless, it is clear that some kind of adjustment to the torsional potential is required, particularly for the α angle of stilbene, and thus the dashed gray lines in Figures 3 and 4 and the second column in Table 2 display the results of the approach described above. We adjusted the OPLS-2005 torsion parameters to better approximate the torsion potentials for the unsubstituted molecules and applied the same adjustments to their substituted derivatives (see Method Details).

For the unsubstituted stilbene torsions, the barrier height is reduced to match the LMP2 result when using what we term the "OPLS-T" force field (OPLS with torsional adjustment). The torsion potentials for α and β resulting from this OPLS-T force field are nearly identical to the LMP2-derived curves. For the unsubstituted bithiophene torsion, γ, a slight adjustment was made to narrow the peak, but the match to the LMP2 curve is very good with either the OPLS-2005 or the OPLS-T force field.

However, for the substituted derivatives of both stilbene and bithiophene, it is clear that these adjustments alone are not sufficient. Although the OPLS-T-calculated barrier heights for stilbene derivatives are an improvement over the OPLS-2005-calculated heights, the substantial discrepancies near 0° remain and even become larger in a few cases, trends that can also be seen in the RMSD values in Table 2. For the substituted bithiophene derivatives, in keeping with the very minor adjustments that were made to the γ torsion potential, almost no differences are seen between the OPLS-2005 and OPLS-T curves, and thus their discrepancies with the LMP2-derived curve persist. It is clear that, in addition to changes in the torsional parameters, other adjustments to OPLS-2005 will be needed in order to properly model these molecules.

It should be noted here, however, that the required torsional potential adjustment depends on other adjustments made to the potential. Thus, in the subsequent sections, as we test additional changes to the OPLS-2005 potential, we refit the torsion to the unsubstituted case after each additional adjustment. So by "OPLS-X-T" we denote the OPLS-2005 potential with an adjustment made to X followed by an adjustment of the torsional potential that results in its fitting to the LMP2-calculated potential for the unsubstituted stilbene and bithiophene torsions; i.e., "T" here indicates some adjustment to the torsion potential, but the precise nature of the adjustment depends on any other changes that have also been made to the standard OPLS-2005 force field. The final set of torsion parameter adjustments for each case is given in Table 3. All torsional adjustments were made simply by varying the V_i

Table 3. Adjustments to the Torsion Parameters for the Various OPLS Potentials

torsions	OPLS-2005	OPLS-T	OPLS-SB-T	OPLS-SB-B14-T
		α angle ??−CM−CM−??[a]		
V_1	0.000	0.000	0.000	0.000
V_2	14.000	10.200	10.200	10.200
V_3	0.000	0.000	0.000	0.000
V_4	0.000	−1.200	−1.200	−1.200
		β angle CM−CM−CA−CA		
V_1	0.316	0.316	0.316	0.316
V_2	3.707	3.350	3.000	3.000
V_3	−0.974	−0.974	−0.947	−0.947
V_4	0.000	−0.100	−0.200	−0.200
		γ angle SA−CA−CA−CA		
V_1	0.276	0.276	0.276	0.276
V_2	1.234	1.234	1.234	1.234
V_3	0.376	0.376	0.376	0.376
V_4	0.000	−0.200	−0.200	−0.200
		γ angle SA−CA−CA−SA		
V_1	1.241	1.241	1.241	1.241
V_2	−1.098	−1.098	−1.098	−1.098
V_3	0.681	0.681	0.681	0.681
V_4	0.000	0.200	0.200	0.200

[a]"??" denotes undefined atom types.

parameters within the standard functional form for the OPLS torsion potential,

$$U(\omega) = \frac{1}{2}V_1(1 + \cos\omega) + \frac{1}{2}V_2(1 - \cos 2\omega) + \frac{1}{2}V_3(1 + \cos 3\omega) + \frac{1}{2}V_4(1 - \cos 4\omega)$$

where ω is the torsion angle and V_1, V_2, V_3, and V_4 are the adjustable parameters.

6.2. Bond-Stretching and Angle-Bending Adjustments. Results from ongoing work at Schrödinger to improve the OPLS force field indicate that bond stretching and angle bending restraints may be unrealistically stiff.[28] Indeed, we plotted the OPLS-2005 energy components for methyl-substituted stilbene and the two methyl-substituted bithiophenes, and the results indicate that angle bending and bond stretching energies both increase at very small torsion angles. As expected, the steric energy also increases at these angles, and jointly, these trends suggest that this increased steric strain is distributed among different degrees of freedom; i.e., bonds are stretching and angles are bending in order to avoid costly steric clashes. If the constraints on these stretches and bends are too stiff, inappropriately high energies will result. On the basis of the observations at Schrödinger as well as our own investigations, we decreased the stretching and bending force constants by 30% and minimized the stilbene and bithiophene derivatives according to this new potential. We also slightly increased the ideal values of two particular angles in the stilbene structures (those included in the α dihedral, see Figure 1), after visual comparisons of the OPLS-2005- and B3LYP-minimized structures indicated that these angles were consistently smaller in the OPLS-2005 versions, bringing the rings into closer contact (see Method Details for details).

We entitle this new potential "OPLS-SB-T," and the corresponding results are represented in Figures 3 and 4 by a dotted orange line. The RMSD values between these OPLS-SB-T results and those from LMP2 are recorded in the third column of Table 2.

Stilbene Derivatives. With these adjustments to the bond-stretching and angle-bending parameters, substantial improvements are obtained in the match between the OPLS-derived and LMP2-calculated β potential energy curves for all substituted stilbene derivatives, with an average improvement of 0.4 kcal/mol in the RMSD values as compared to the OPLS-T results. In addition, all but one of the OPLS-SB-T-derived β potential energy curves are within chemical accuracy, that is, within 1.0 kcal/mol of the LMP2-derived values. It is clear in Figure 3e that the OPLS-SB-T potential results in marked improvements over both the OPLS-2005 and OPLS-T potentials. The one case that remains outside of chemical accuracy, with an RMSD value of 1.08 is that where R = OH (we discuss this case further in section 7).

Bithiophene Derivatives. Substantially more accurate results are obtained using the OPLS-SB-T potential for these molecules as well, with an impressive 0.6 kcal/mol average decrease in the RMSD between the LMP2 and OPLS-SB-T derived potential energy curves. The results for two bithiophene derivatives, 3,3′-diethyl-bithiophene and 3,3′-diisopropyl-bithiophene, remain outside chemical accuracy. However, the decreases in RMSD for these two species were actually the most substantial in the set, with a decrease of 1.0 kcal/mol for the former and 1.2 kcal/mol for the latter.

Although the adjustments to OPLS-2005 described in this section are by no means a permanent solution, the improvements made by this simple heuristic approach are impressive. In addition, they are easily implemented and can serve as a simple fix for such problems until the time when these stretching and bending force constants have been recalculated and reassigned in a more comprehensive fashion.

6.3. Steric Repulsion Adjustments. The repulsive part of the standard 12−6 Lennard-Jones (LJ) potential has long been known to overestimate the repulsive forces at very short interatomic distances.[29,30] However, due to the ease of its calculation, this functional form has found its way into nearly all classical modeling potentials. Since biomolecular systems under reasonable temperatures and pressures do not often access the problematic region of the LJ potential, it is usually an acceptable approximation. However, as previously discussed, in conjugated polymers the joint effects of shorter bond lengths along the main chain and conjugation-induced planarity combine to force a small set of atoms into closer-than-usual contact.

Experimental deviations from the LJ 12−6 potential at short interparticle distances have been well-documented for molecular hydrogen[31] as well as for the noble gases.[32] These deviations begin around $0.8r_{min}$, where r_{min} is the optimal interatomic distance in the standard LJ potential, and quickly become substantial as interatomic distances decrease further.[31,32] In our B3LYP-minimized structures, atoms of the substituted side chains frequently come into closer than $0.8r_{min}$ contact with the atoms of the main chain in the near-planar configurations, suggesting that the LJ potential may be inadequate for these polymers.

We therefore consider the buffered 14−7 potential, which, according to the analysis of experimentally derived interatomic potentials for the noble gases, provides the best approximation of the true repulsive potential while keeping the attractive potential acceptably close to that described by the LJ function.[32]

dx.doi.org/10.1021/ct300175w | J. Chem. Theory Comput. 2012, 8, 4556−4569

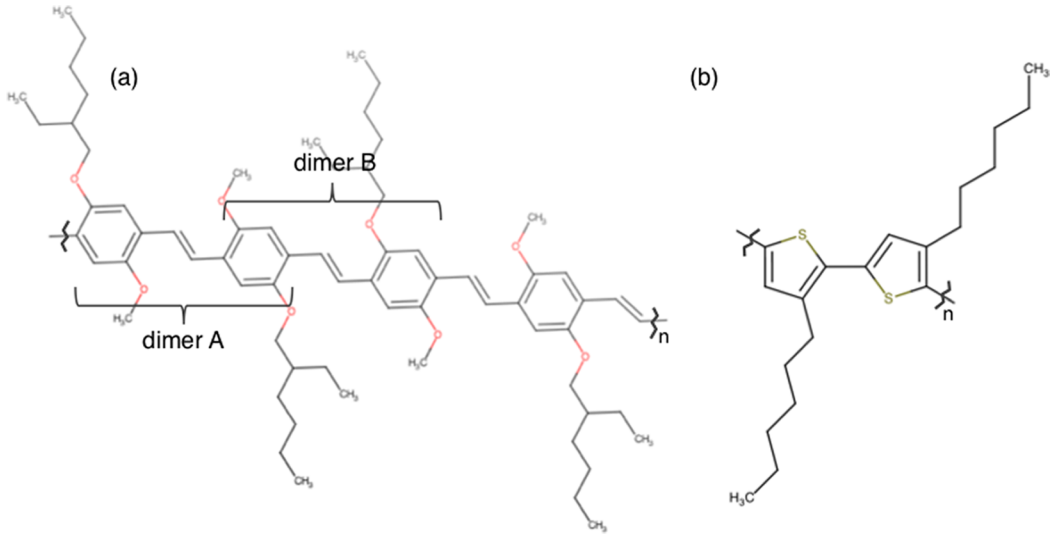

Figure 5. The structures of (a) MEH-PPV and (b) P3HT. Note that there are two options (A and B) for the side-chain configurations within an MEH-PPV dimer.

The buffered 14−7 potential can be written as

$$U(r) = \varepsilon\left(\frac{1.07r_{min}}{r + 0.07r_{min}}\right)^7\left(\frac{1.12r_{min}^7}{r^7 + 0.12r_{min}^7} - 2\right)$$

where r_{min} is the interatomic distance at which the potential is at its minimum and ε is the value at that minimum.

Results for this new potential, "OPLS-SB-B14-T," are shown in Figures 3 and 4, indicated by a solid red line, and the RMSD values between these results and those from LMP2 are recorded in the last column of Table 2.

As can be seen both in Table 2 and in Figures 3 and 4, the improvement to the potential energy curves resulting from the use of the buffered 14−7 potential is somewhat minimal. For the substituted stilbenes, its implementation actually worsens the match between the OPLS- and LMP2-derived potentials, albeit very slightly, with an average increase of 0.02 kcal/mol in RMSD as compared to that of the OPLS-SB-T potential. However, for the substituted bithiophenes, improvements in the match are seen in all cases, and there is an average decrease of 0.19 kcal/mol in the RMSD values. Although modest, the largest improvements occur in the near-planar configurations, where the LMP2- and OPLS-derived potentials deviate the most. As a result, for the purposes of this paper, we include this adjustment in our potential, despite its modest effect. However, as most of the improvements are gained without it, and further testing would be needed to determine if the buffered 14−7 potential would yield improvements in other systems, we consider this adjustment to the OPLS potential optional. (It should be noted that the same torsional adjustments are made to both the OPLS-SB-T and OPLS-SB-B14-T potentials, as shown in Table 3, and can thus be used with either the buffered 14−7 or the standard LJ potential.)

7. OPLS-SB-B14-T-CALCULATED POTENTIALS

With the OPLS-SB-B14-T potential, we are able to reproduce, within chemical accuracy, the results of the LMP2 calculations for all except four of the torsion potentials considered. The final average reduction in error between the LMP2- and the OPLS-derived potentials was 1.02 kcal/mol, and much of this reduction occurred in the low-angle region, precisely where the largest initial differences between the LMP2 and OPLS-2005 results were found. The four torsion potentials that deviate the most from the LMP2 results when calculated with OPLS-SB-B14-T also had the largest deviations when calculated with OPLS-2005, and the final OPLS-SB-B14-T-derived RMSD values demonstrate significant improvements (see Table 2). Importantly, the OPLS-optimized structures differ only minimally from the B3LYP-optimized ones with average structural RMSDs of 0.17 Å and 0.18 Å, when optimizing with OPLS-2005 and OPLS-SB-B14-T, respectively. (Averages were calculated over RMSDs for the 0°, 90°, and 180° structures of all torsions in Figures 3 and 4.)

The hydroxyl-substituted stilbene case deserves additional discussion. Compared to the curves of the other substituted stilbenes in Figure 3, the R = OH case remains an outlier—both the barrier and the low-angle portion of the LMP2 curve are poorly reproduced by the OPLS-SB-B14-T potential. After close examination of the minimized structures, we hypothesize that the polar hydroxyl group may induce polarization to differing degrees as it rotates around the β dihedral angle. To test this hypothesis, we calculated the atomic charges from the electrostatic potential at the B3LYP/cc-pVQZ(-G) level. The results indicate that the charges on the hydrogens in the inter-ring linker region vary substantially with the β angle rotation. As the torsion approaches 0°, where the oxygen atoms of both OH groups are positioned close to one of the linker hydrogens, the charge on that hydrogen atom becomes more positive by about 60%, decreasing the energy of these low-angle conformations. Unfortunately, this kind of configuration-dependent polarization effect cannot be fully modeled within the limits of a nonpolarizable potential.

8. MD SIMULATIONS

Using both the OPLS-2005 and the OPLS-SB-B14-T potentials, we performed MD simulations for polymers of P3HT (10 monomers in length) and MEH-PPV (60 monomers in length), two of the most widely studied conjugated polymers (see Figure 5). We then examined the resulting trajectories for several features: their torsion angle distributions, persistence lengths, and conjugation length distributions. The lengths of the polymers investigated were

intentionally chosen to approximate their persistence lengths. As a result, the polymers remained extended throughout the simulations, and complications arising from self-attraction and self-avoidance between disparate parts of the polymer were avoided. Additional simulation and analysis details can be found in the Method Details section.

8.1. Torsion Angle Distributions. Shifts in the distribution of sampled dihedral angles are clearly expected to result from the changes that differentiate OPLS-SB-B14-T from OPLS-2005, as these changes were designed to adjust the relative energies of these angles. Nevertheless, the distribution shifts for commonly modeled polymers serve to illustrate the effect of these adjustments. The OPLS-2005 and OPLS-SB-B14-T potential energy curves for the α and β torsions of MEH-PPV dimers and the γ torsion of the P3HT dimer are shown in Figure 6, while their sampled distributions during our MD simulations are shown in Figure 7.

As expected from the curves plotted in Figure 6a, the distribution of sampled MEH-PPV α angles broadens when modeled with the OPLS-SB-B14-T potential. However the range of angles remains quite restricted, since the barrier between *cis* and *trans* configurations, although less than in

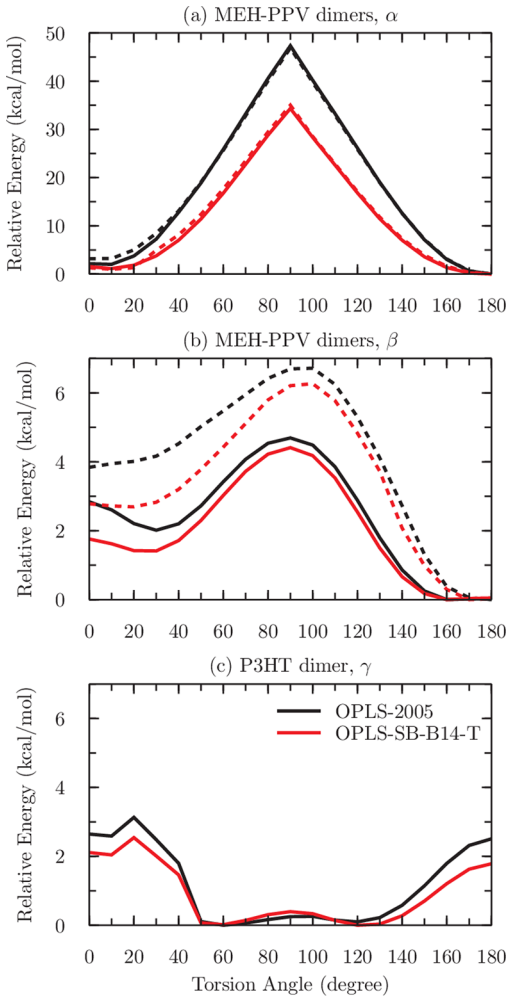

Figure 6. Comparison between the OPLS-2005 and OPLS-SB-B14-T potentials for (a) the α and (b) the β torsion angles of an MEH-PPV dimer, as well as (c) the γ torsion of a P3HT dimer. The solid lines in (a) and (b) represent the results for dimer A, while the dashed lines represent those for dimer B (see Figure 5).

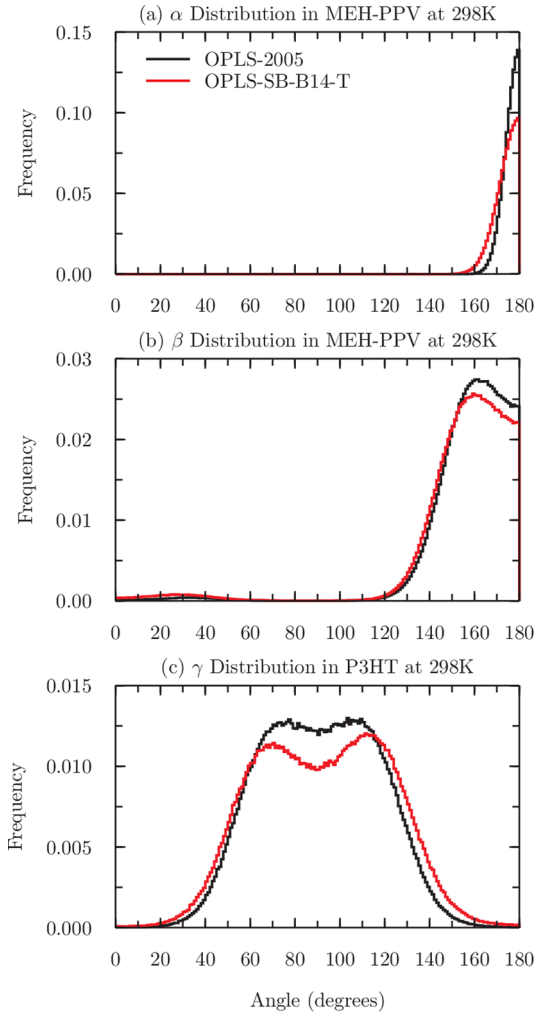

Figure 7. Comparison of dihedral angle distributions from MD simulations using OPLS-2005 and OPLS-SB-B14-T for (a) the α angle of MEH-PPV, (b) the β angle of MEH-PPV, and (c) the γ angle of P3HT.

OPLS-2005, remains greater than 30 kcal/mol. All α dihedrals were initialized in the *trans* configuration, and the barrier appears insurmountable at our sampling temperature (295 K). Similarly, the distribution of MEH-PPV β angles slightly broadens as expected with the use of the OPLS-SB-B14-T potential. Importantly, the population at small angles increases substantially over the population that is present when modeled with OPLS-2005, demonstrating the conformational bias that results from an overestimation of the energy in this region, see Figure 6b.

Finally, the distribution of P3HT γ angles also broadens with the implementation of OPLS-SB-B14-T. In this case, the likelihood of near-planar configurations with both large and small angles increases substantially, see Figure 6c.

8.2. Persistence Lengths. In modeling the behavior of long stretches of these polymers, it is important to properly represent their flexibility, especially when probing folding behaviors. We therefore calculated the persistence lengths of single, extended stretches of MEH-PPV and P3HT. The persistence length (L_p) is the contour length over which correlations in the polymer's orientation persist (see Method Details for details). Results indicate nearly identical persistence lengths for both OPLS-2005 and OPLS-SB-B14-T potentials.

dx.doi.org/10.1021/ct300175w | J. Chem. Theory Comput. 2012, 8, 4556−4569

For MEH-PPV, we calculated persistence lengths of 53 ± 4 monomers using OPLS-2005 and 51 ± 2 monomers using OPLS-SB-B14-T. Increased rotations around the α torsion would be expected to result in a shorter L_p, but the slight broadening of values observed in the OPLS-SB-B14-T model (see Figure 7a) appears insufficient to effect a statistically significant decrease in L_p. In contrast, changes to the rotations around the β angle are not expected to alter L_p; since the bond to the adjacent monomer lies along the β torsion's rotational axis, the direction of the polymer does not meaningfully change with β angle rotations.

Experimental measurements of L_p range from 9 to 50 monomers for MEH-PPV.[33−36] However, the shorter-length values are derived from experiments on MEH-PPV polymers that most likely contained a substantial fraction of *cis* vinyl linkages and tetrahedral defects (where a single bond replaces the double bond in the vinyl group).[33−35] Depending on the synthetic method, *cis* and tetrahedral defects can each occur at up to 5% of the interphenyl linkages.[37−40] Since the persistence length is heavily influenced by such defects,[35] these shorter measurements are likely more reflective of the average distance between defects than the true stiffness of an all-*trans*, defect-free stretch of MEH-PPV. In contrast, the longest experimental estimate, 50 monomers,[36,41] is derived from vibrational spectra of individual stretching and bending modes in PPV and thus provides a better estimate of its true stiffness (neglecting, however, the influence of the MEH side chains). Its correspondence to our calculated L_p is striking.

For P3HT, L_p was found to be 8.8 ± 0.9 monomers using OPLS-2005 and 8.7 ± 0.4 monomers using OPLS-SB-B14-T. The degree of rotation around the γ angle has a potentially significant effect on the persistence length, especially if the near-planar configurations are heavily favored. However, these rotations access a wide range of angles with both OPLS potentials, and therefore it is not surprising that we observe no change, especially given the shorter L_p. Experimental estimates of L_p for P3HT range from 6.2[42] to 8.6[43] monomers. As polythiophenes lack the kind of structural complications described above for PPVs, these measurements do represent the true polymer stiffness, and our calculated L_p, though slightly longer, is comparable.

8.3. Conjugation Length Distributions. The conjugation length is the length over which the π electrons are delocalized in a conjugated system. Since a chromophore's electronic properties depend upon its length, understanding the distribution of conjugation lengths within a polymer is essential for understanding its behavior as a semiconductor. Although the extent of potential conjugation, i.e., the length over which alternating single and double bonds extends, is sometimes used as a proxy for this conjugation length, the true conjugation length, L_c, can be shorter as a result of conformational variations that inhibit delocalization. In order for electrons to delocalize, p orbitals on the different atoms must be approximately coplanar, and thus rotations around conjugated bonds that break the planarity of the conjugated segment can also cause a break in conjugation. Rotations of greater than 40° from planarity have been found to induce changes in electronic properties,[44] and this cutoff has proven useful in estimating the extent of conjugation.[45] Using this metric, we calculated the distributions of conjugation lengths in MEH-PPV and P3HT during our MD simulations.

For MEH-PPV, the conjugation lengths in our simulations ranged from shorter than one monomer to the entire length of the 60-unit polymer, for both OPLS-2005 and OPLS-SB-B14-T potentials. Figure 8a shows the distribution of L_c values. With

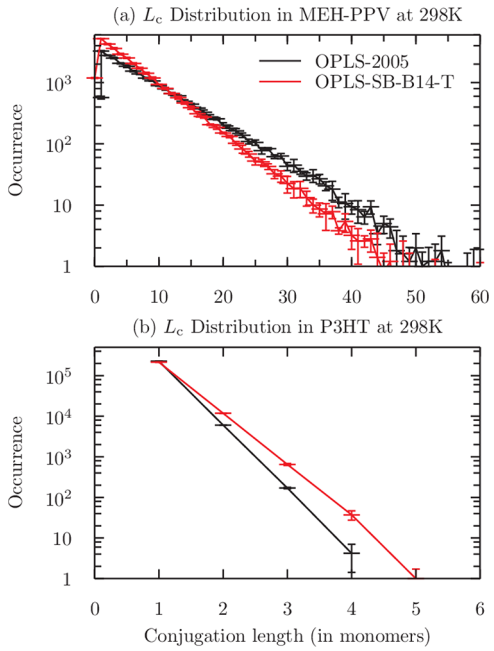

Figure 8. Comparison of conjugation length distributions from MD simulations using OPLS-2005 and OPLS-SB-B14-T for (a) MEH-PPV and (b) P3HT.

the adjustments included in OPLS-SB-B14-T, the distribution shifts toward shorter conjugation lengths, and the average L_c is 5.6 monomers as compared to 7.2 monomers when the OPLS-2005 potential is used. We note, however, that in experiments with most MEH-PPV polymers, the presence of the tetrahedral and *cis* defects will impose additional limits on L_c.

For P3HT, very short conjugation lengths of just one monomer dominate the distributions, with average L_c values of 1.03 and 1.06 monomers for the OPLS-2005 and OPLS-SB-B14-T potentials, respectively. However, the dominance of single-monomer chromophores masks the substantial differences seen in the distributions of L_c values beyond this length (see Figure 8b). In fact, the frequency of segments with a two-monomer L_c doubles with the changes implemented in OPLS-SB-B14-T, while the frequency of conjugated segments extending for three or more monomers nearly quadruples.

It is important to note that for both MEH-PPV and P3HT, the self-association known to occur in condensed phases[16,38] will greatly influence the distributions of these conjugation lengths. Polythiophenes, in particular, are known to form extended crystals with nearly coplanar rings.[16] However, the additional forces present in the dense crystalline environment build upon the intrinsic intermolecular forces, and it is clear from our analysis that even relatively small shifts in the dihedral angle distributions can have substantial effects when modeling the structural properties that influence electronic behaviors.

9. CONCLUSION

In this work, we have assessed the accuracy of a variety of classical force fields in modeling the constituents of PPV- and PT-based conjugated polymers. We then made adjustments to the OPLS-2005 force field in order to improve its modeling of the inter-ring torsion potentials of a series of substituted

stilbene and bithiophene derivatives. Our new potential, OPLS-SB-B14-T, is based on the standard OPLS-2005 potential but contains adjustments to the torsion, bond-stretching, and angle-bending parameters, while also utilizing the buffered 14−7 potential to better approximate the steric repulsions at very close interatomic distances. These changes result in substantial improvements in the correspondence between the adjusted OPLS- and LMP2-derived torsional potential energy curves for two very different conjugated polymers with a variety of substituted side-chain groups. That these improvements were obtained for several different molecules with the same OPLS-SB-B14-T force field demonstrates this potential's transferability and suggests that it should be applicable to other conjugated systems as well (although adjustments would have to be made to additional torsional parameters if the molecule contained main-chain dihedral angles other than those adjusted here). Our results also suggest that the corrections applied here may be necessary to appropriately model other systems where very short interatomic distances are encountered. Finally, we note that, with the exception of the optional buffered 14−7 potential (see section 6.3), the OPLS corrections proposed here require only simple adjustments to the OPLS parameter files. While work is underway at Schrödinger to provide a more comprehensive overhaul of these parameters for a wide range of conjugated moieties, the adjustments presented here allow us to more accurately explore the structural and electronic behaviors of PT- and PPV-based conjugated polymers.

Even very accurate classical force fields, however, will at some level prove inadequate at reproducing the forces acting within a given molecule, and in order to anticipate when and how the behavior of a modeled system will deviate from that of the physical one, we must understand the types of errors expected. Our investigations of different substituent groups and a variety of force field variations have led us to an understanding of the types of errors that may be expected when using OPLS-like force fields to model these polymers (see Figures 3 and 4). In particular, we have learned that conformational change may significantly affect polarization in ways the OPLS-based potential is unable to replicate. Nevertheless, the improvements obtained with the OPLS-SB-B14-T potential enable us to more accurately model the energy basins and barriers of the inter-ring torsion potential, particularly for near-planar configurations, and to more accurately compare the behavior of polymers with different side chains.

Our adjustments to the OPLS-2005 potential result in observable, if somewhat minor, shifts in dihedral angle populations during gas-phase MD simulations of P3HT and MEH-PPV. However these shifts did not translate into observable differences in persistence lengths. While these equilibrium properties may not look dramatically changed as a result of the OPLS modifications, barriers are substantially altered, as are the relative energies of planar and nonplanar states. As a result, dynamical fluctuations will be sensitive to these more accurate potentials, and more substantial differences are to be expected in folding and assembly behaviors and excursions into higher energy configurations, such as fluctuations into and out of planar configurations. This last property is particularly important for understanding absorption, emission, and energy transfer within conjugated polymers, all of which are heavily influenced by these structural features. And, indeed, we do observe a far more substantial difference in the OPLS-2005 and OPLS-SB-B14-T calculated distributions of conjugation lengths (note the log scale in Figure 8). An accurate modeling of these conjugation lengths is particularly important in techniques that couple quantum mechanical approaches to classical force fields in order to investigate excitations and charge transfer; such techniques may prove especially attractive in elucidating the functional properties of conjugated polymers.

Theoretical investigation into the semiconducting nature of conjugated polymer materials requires a multiscale approach. Electron delocalization depends on molecular-scale details such as the degree of inter-ring twisting, while bulk transport efficiencies depend on polymer folding, aggregation, and the presence of grain boundaries between well-ordered regions. Appropriate modeling at the molecular level allows us to probe some of these features while facilitating the development of accurate coarse-grained models with which to probe longer times and larger systems.

10. METHOD DETAILS

10.1. QM Calculations. All geometries were optimized at the B3LYP/6-31+G** level, followed by single-point calculations at the LMP2/cc-pVTZ(-f) level within Jaguar v. 7.6.[9] In stilbene, there are two symmetrically equivalent β bonds. Therefore, in all geometry optimizations, one of these torsions was held at 0°, while the other was sampled at 0°, 10°, ..., 170°, and 180°.

Electrostatic potential (ESP) single-point calculations were performed on all stilbene geometries with R = OH to test the effect of torsion angle on the polarization of those geometries obtained at the B3LYP/6-31+G** level. These calculations were performed using B3LYP with various basis sets (cc-pVDZ, cc-pVTZ, cc-pVQZ(-G)) to test for conversion of ESP with increasing size of the basis. Finally, the ESPs calculated at the B3LYP/cc-pVQZ(-G) level were used to calculate the atomic charges.

All canonical MP2 calculations were performed with QChem,[46] as Jaguar does not have canonical MP2 capabilities. Single point calculations were done using the frozen core approximation and were done in serial. The nonstandard cc-pVTZ(-f) basis set was obtained by including a *basis* section in the QChem input file where the set of *f* functions was removed from the set of all functions on the carbon atom, i.e., four *s* functions, three sets of *p* functions, two sets of *d* functions, and one set of *f* functions, the latter being removed. For stilbene and the methyl-substituted stilbene in the cc-pVTZ(-f) basis set, there are 490 and 694 functions respectively, and we found that the default QChem memory and disk settings were sufficient. Calculations employing the cc-pVQZ basis set for stilbene (1130 basis functions) required greater resources than the default. We were unable to obtain cc-pVQZ results for the methyl-substituted stilbene (1590 basis functions) even when using a variety of heavy duty memory and disk options as well as different algorithms for the MP2 integral transformation.

10.2. Molecular Mechanics Calculations. Starting with the QM-optimized geometries, structures were minimized using the OPLS-2005 potential as well as the OPLS-T, OPLS-SB-T, and OPLS-SB-B14-T potentials. As described above, torsions were sampled every 10° from 0° to 180°, and in stilbene, one β angle was held fixed at 0° while the other was rotated. Minimizations were performed using MacroModel[25] (for Figure 2) and in-house Schrödinger software (for Figures 3, 4, and 6) with no interaction cutoffs and the dielectric constant set to 1.0. We used the 10° B3LYP-minimized structure as the initial configuration for the OPLS-minimization of 3,4′-

dimethyl-bithiophene structures at 0°, as the 0° B3LYP-minimized structure appeared to be caught in a false minimum on the OPLS potential energy surface. In addition, we restrained four dihedral angles within the long, floppy side chains of the MEH-PPV and P3HT dimers in order to obtain a smooth potential. The restrained dihedral angles were chosen so that the side chains remained pointed out into space and therefore did not clash during rotation. Since LMP2-minimized structures were unavailable for these dimers, optimizations were begun from structures that had been previously optimized with OPLS-2005. The MM3* potential used in Figure 2 differs slightly from that of MM3 as derived by Lii and Allinger[20] in that it uses partial charges instead of bond dipoles, improper torsions for out-of-plane bending, and specific, static, torsional terms for conjugated systems without an iterative SCF bond order calculation.[25]

Torsion Adjustments. Incremental adjustments were made manually to the V_1, V_2, V_3, and V_4 torsion parameters until a good match was obtained to the QM-derived curves for unsubstituted stilbene (for the α and β angles) and for unsubstituted bithiophene (for the γ angle). Adjustments for the OPLS-SB-T and OPLS-SB-B14-T potentials were made as the last step after all other adjustments. Table 3 shows the final values of these parameters for each potential.

Bond-Stretching and Angle-Bending Adjustments. A small increase was made to the ideal value of the CA−CM−CM angle, where CA and CM are atom types within OPLS. (This angle is included in the α dihedral, see Figure 1), from 123.66° to 128.30°. In addition, all stretching and bending force constants were reduced by 30%. These adjustments were motivated by our comparisons of the QM-minimized and OPLS-2005-minimized structures as well as by preliminary results at Schrödinger. The specific values were chosen after investigations demonstrated their utility in improving the resulting match to the QM-derived potential energy curves.

Steric Repulsion Adjustments. The buffered 14−7 potential was introduced instead of the LJ 12−6 potential based on previous work, demonstrating that it more accurately approximates the steric repulsions between noble gases at very short interatomic distances.[32] Several other adjustments to the repulsive part of the LJ potential were also tested, but only those that resulted in an unacceptably soft potential appeared to substantially improve the match to the QM results. It is important to note that the r_{min}/σ ratio is 0.18% larger for the buffered 14−7 than the LJ 12−6. We used the same σ values for both potentials, and the r_{min} values are computed accordingly.

Comparisons to QM Potentials. Comparisons were made between the LMP2- and the OPLS-derived potential energy curves through the use of visual inspection (see Figures 3 and 4) and RMSD quantification (see Table 2).

10.3. MD Simulations. MD simulations of P3HT and MEH-PPV polymers were run using both OPLS-2005 and OPLS-SB-B14-T within TINKER.[47] The P3HT molecules were 10 monomers in length and regioregular, with all head-to-tail linkages (as represented by the 3,4′-disubstituted bithiophenes). The MEH-PPV molecules were 60 monomers in length, with regioregular, syntactic side-chain placement. Polymer lengths were chosen so that the polymers remained extended throughout the simulations in order to avoid complications from self-attractions and self-avoidance in our measured quantities. Each simulation consisted of a single polymer in the gas phase.

OPLS-2005 and OPLS-SB-B14-T parameter input files were created for TINKER with the use of in-house Schrödinger software. Sampling was done within the NVT ensemble at 298 K, using the velocity verlet algorithm with 2 fs timesteps and an Andersen thermostat. A dielectric constant of 1.0 was used, and tapered cutoffs were implemented from 10.8 to 12.0 Å for the van der Waals attractions and from 7.8 to 12.0 Å for the electrostatic interactions. Although cutting off the electrostatic potential always results in the loss of a significant portion of the electrostatic energy, we observed that the effect of this cutoff on the differences in energy between various polymer configurations was minimal—even smaller, in fact, than the effect of introducing reasonable periodic boundary conditions and using Ewald summation to approximate the long-range electrostatic contributions. Thus, it appears that, for our purposes of sampling a variety of extended configurations, implementing such a cutoff in the electrostatic potential is acceptable. Previous simulations on conjugated polymers also make use of this approximation.[16]

Five trials of P3HT were run for 120 ns each, with atomic positions collected for analysis every 5 ps. For MEH-PPV, 25 trials were run for 6 ns each, and atomic positions were collected every 10 ps. All runs started from different extended configurations generated during an equilibration run after at least 0.5 ns. Each set of simulations was run twice, once using OPLS-2005 and once using OPLS-SB-B14-T.

Calculations of L_p. Persistence lengths were determined by fitting the decay in polymer orientation to the following relation:

$$\langle \cos \theta_{i,i+j} \rangle = \exp(-S_j/L_p) \quad (1)$$

where $\theta_{i,i+j}$ is the angle between vectors tangent to the polymer at monomers i and $i + j$, S_j is the contour length between monomers i and $i + j$ (i.e., the length of the polymer segment that connects monomers i and $i + j$), and L_p is the persistence length. Tangent vectors were defined as running from the start of one monomer to the start of the next. j was varied from 0 to 9 monomer units for P3HT and 0 to 10 for MEH-PPV. Multiple points were collected from each polymer configuration; i.e., the averaging of cos θ ran both over different configurations as well as over different i positions. For P3HT, the persistence length was fit separately for each MD trial, and the average and standard deviation values were calculated across these five trials. For MEH-PPV, the persistence length was fit separately for five groups, each of which included data from five independent MD runs, and the average and standard deviation values were calculated across these five groups.

Calculations of Dihedral Angle Distributions. Dihedral angles were collected from all output configurations from all runs, binned in 1° increments, and plotted in Figure 7.

Calculations of L_c. Conjugation lengths were determined by measuring the dihedral angles between moieties that would ideally be coplanar when conjugated. For P3HT, only γ was considered (see Figure 1b). For MEH-PPV, three angles were considered: two β and α (see Figure 1a). Conjugation lengths were then gathered from all configurations and binned in one-monomer increments (with each of the three angles in MEH-PPV contributing an appropriate fraction of a monomer). Histograms were calculated separately for the five trials of P3HT and the five groups of five trials each for MEH-PPV so that error bars could be determined for the histogram values. Figure 8 presents these averaged histograms.

AUTHOR INFORMATION

Corresponding Author

*E-mail: rich@chem.columbia.edu.

Present Addresses

[§]Schrödinger, New York, New York, United States.

[∥]Novartis Institutes for Biomedical Research, Cambridge, Massachusetts, United States.

Notes

The authors declare the following competing financial interest(s): R. Friesner has a significant financial stake in Schrodinger, Inc., is a consultant to Schrodinger, Inc., and is on the Scientific Advisory Board of Schrodinger, Inc..

ACKNOWLEDGMENTS

We would like to thank Ed Harder and Schrödinger, Inc., for helpful discussions and the use of in-house software. In addition, we would like to thank Kyle Plunkett at Southern Illinois University Carbondale for his insight into synthetic methods. This work was supported as part of the program "Molecular Tools for Conjugated Polymer Analysis and Optimization," a Center for Chemical Innovation (CCI, phase 1) under NSF Award No. CHE-0943957.

REFERENCES

(1) *Basic Research Needs for Solar Energy Utilization: Report of the Basic Energy Sciences Workshop on Solar Energy Utilization April 18−21, 2005*; Office of Science, U.S. Department of Energy: Washington, DC, 2005.

(2) Sirringhaus, H.; Brown, P. J.; Friend, R. H.; Nielsen, M. M.; Bechgaard, K.; Langeveld-Voss, B. M. W.; Spiering, A. J. H.; Janssen, R. A. J.; Meijer, E. W.; Herwig, P.; de Leeuw, D. M. *Nature* **1999**, *401*, 685−688.

(3) Murphy, R. B.; Beachy, M. D.; Friesner, R. A.; Ringnalda, M. N. *J. Chem. Phys.* **1995**, *103*, 1481−1490.

(4) Saebo, S.; Pulay, P. *J. Chem. Phys.* **1987**, *86*, 914−922 914−922..

(5) Dunning, T. H. *J. Chem. Phys.* **1989**, *90*, 1007−1023.

(6) Kendall, R. A.; Dunning, T. H.; Harrison, R. J. *J. Chem. Phys.* **1992**, *96*, 6796−6806.

(7) Woon, D. E.; Dunning, T. H. *J. Chem. Phys.* **1993**, *98*, 1358−1371.

(8) Woon, D. E.; Dunning, T. H. *J. Chem. Phys.* **1994**, *100*, 2975−2988.

(9) *Jaguar*, version 7.6.; Schrodinger, LLC: New York, 2009.

(10) Kaminski, G. A.; Friesner, R. A.; Tirado-Rives, J.; Jorgensen, W. L. *J. Phys. Chem. B* **2001**, *105*, 6474−6487.

(11) Kaminski, G. A.; Maple, J. R.; Murphy, R. B.; Braden, D. A.; Friesner, R. A. *J. Chem. Theory Comput.* **2005**, *1*, 248−254.

(12) Wang, L.; Berne, B. J.; Friesner, R. A. *Proc. Natl. Acad. Sci. U. S. A.* **2012**, *109*, 1937−1942.

(13) Raos, G.; Famulari, A.; Marcon, V. *Chem. Phys. Lett.* **2003**, *379*, 364−372.

(14) Kwasniewski, S. P.; Claes, L.; Francois, J.-P.; Deleuze, M. S. *J. Chem. Phys.* **2003**, *228*, 7823−7836.

(15) van Hutten, P. F.; Wildeman, J.; Meetsma, A.; Hadziioannou, G. *J. Am. Chem. Soc.* **1999**, *121*, 5910−5918.

(16) Moreno, M.; Casalegno, M.; Raos, G.; Meille, S. V.; Po, R. *J. Phys. Chem. B* **2010**, *114*, 1591−1602.

(17) Darling, S. B.; Sternberg, M. *J. Phys. Chem. B* **2009**, *113*, 6215−6218.

(18) Jorgensen, W. L.; Maxwell, D. S.; Tirado-Rives, J. *J. Am. Chem. Soc.* **1996**, *118*, 11225−11236.

(19) Banks, J. L.; et al. *J. Comput. Chem.* **2005**, *26*, 1752−1780.

(20) Lii, J.-H.; Allinger, N. *J. Am. Chem. Soc.* **1989**, *111*, 8551−8566.

(21) Marcon, V.; Raos, G. *J. Phys. Chem. B* **2004**, *108*, 18053−18064.

(22) Sumpter, B. G.; Kumar, P.; Mehta, A.; Barnes, M. D.; Shelton, W. A.; Harrison, R. J. *J. Phys. Chem. B* **2005**, *109*, 7671−7685.

(23) Marcon, V.; Raos, G. *J. Am. Chem. Soc.* **2006**, *128*, 1408−1409.

(24) Adachi, T.; Brazard, J.; Ono, R. J.; Hanson, B.; Traub, M. C.; Wu, Z. Q.; Li, Z. C.; Bolinger, J. C.; Ganesan, V.; Bielawski, C. W.; Bout, D. A. V.; Barbara, P. F. *J. Phys. Chem. Lett.* **2011**, *2*, 1400−1404.

(25) *MacroModel User Manual*; Schrödinger, LLC: New York, 2008.

(26) Halgren, T. *J. Comput. Chem.* **1996**, *17*, 490−519.

(27) Widge, A. S.; Matsuoka, Y.; Kurnikova, M. *J. Mol. Graphics Modell.* **2008**, *27*, 34−44.

(28) Schrödinger. Unpublished results, 2011.

(29) Slater, J. C. *Phys Rev* **1928**, *32*, 349−360.

(30) Buckingham, R. A. *Proc. R. Soc. London, Ser. A* **1938**, *168*, 264−283.

(31) Silvera, I. F. *Rev. Mod. Phys.* **1980**, *52*, 393−452.

(32) Halgren, T. A. *J. Am. Chem. Soc.* **1992**, *114*, 7827−7843.

(33) Gettinger, C. L.; Heeger, A. J.; Drake, J. M.; Pine, D. J. *J. Chem. Phys.* **1994**, *101*, 1673−1678.

(34) Ou-Yang, W.-C.; Chang, C.-S.; Chen, H.-L.; Tsao, C.-S.; Peng, K.-Y.; Chen, S.-A.; Han, C. C. *Phys. Rev. E: Stat., Nonlinear, Soft Matter Phys.* **2005**, *72*, 031802.

(35) Choudhury, P. K.; Bagchi, D.; Menon, R. *J. Phys.: Condens. Matter* **2009**, *21*, 195801.

(36) Orion, I.; Buisson, J. P.; Lefrant, S. *Phys. Rev. B* **1998**, *57*, 7050−7065.

(37) Becker, H.; Spreitzer, H.; Ibrom, K.; Kreuder, W. *Macromolecules* **1999**, *32*, 4925−4932.

(38) Hu, D.; Yu, J.; Wong, K.; Bagchi, B.; Rossky, P. J.; Barbara, P. F. *Nature* **2000**, *405*, 1030−1033.

(39) Gowri, R.; Mandal, D.; Shivkumar, B.; Ramakrishnan, S. *Macromolecules* **1998**, *31*, 1819−1826.

(40) Bounos, G.; Ghosh, S.; Lee, A. K.; Plunkett, K. N.; DuBay, K. H.; Bolinger, J. C.; Zhang, R.; Friesner, R. A.; Nuckolls, C.; Reichman, D. R.; Barbara, P. F. *J. Am. Chem. Soc.* **2011**, *133*, 10155−10160.

(41) Adachi, T.; Brazard, J.; Chokshi, P.; Bolinger, J. C.; Ganesan, V.; Barbara, P. F. *J. Phys. Chem. C* **2010**, *114*, 20896−20902.

(42) Heffner, G. W.; Pearson, D. S. *Macromolecules* **1991**, *24*, 6295−6299.

(43) Cesar, B.; Rawiso, M.; Mathis, A.; Francois, B. *Synth. Met.* **1997**, *84*, 241−242.

(44) Brédas, J. L.; Street, G. B.; Thémans, B.; André, J. M. *J. Chem. Phys.* **1985**, *83*, 1323−1329.

(45) Bernardi, M.; Giulianini, M.; Grossman, J. C. *ACS Nano* **2010**, *4*, 6599−6606.

(46) Shao, Y.; et al. *Phys. Chem. Chem. Phys.* **2006**, *8*, 3172−3191.

(47) *TINKER 5.1*; Ponder, J. W.; Washington University: St. Louis, MO, 2010.